Talanta 88 (2012) 445–449

Contents lists available at SciVerse ScienceDirect

Talanta

journal homepage: www.elsevier.com/locate/talanta

Synthesis, characterization, and electrochemical applications of carbon nanoparticles derived from castor oil soot

K. Sudhakara Prasad [1], Min-Chieh Chuang [1], Ja-An Annie Ho *

BioAnalytical and Nanobiomedicinal Laboratory, Department of Biochemical Science and Technology, National Taiwan University, No. 1, Sec. 4, Roosevelt Road, Taipei 10617, Taiwan

ARTICLE INFO

Article history:
Received 17 August 2011
Received in revised form 23 October 2011
Accepted 25 October 2011
Available online 9 November 2011

Keywords:
Carbon nanoparticles
Cyclic voltammetry
Modified electrodes
Electrocatalysis

ABSTRACT

A simple procedure for the modification of carbon nanoparticles (CNPs) from castor oil soot using acid treatment was described herein. Characterization studies revealed the presence of edge plane sites and surface carbon–oxygen functionalities at the surface of the CNP material. Voltammetric studies revealed the increased electrochemical activity of the CNP-modified electrode toward various biologically important molecules, including dopamine, uric acid, dihydronicotinamide adenine dinucleotide, tyrosine, and serotonin, relative to those obtained using the unmodified electrode. The improved electro-oxidation potentials for these compounds—and, thereby, the enhanced sensitivity of related sensors—was due directly to the presence of surface C(δ+)═O(δ−) functional groups and the greater number of edge plane sites developed after acid treatment of the soot sample.

1. Introduction

In the last two decades, carbon nanostructures—including fullerenes, carbon nanotubes, and carbon onions (hyperfullerenes)—have become materials of increasing interest because of their unique physical and chemical properties [1–3]. Because of the highly stable graphite structures of these carbon nanostructures, conventional methods of preparation (e.g., chemical vapor deposition, arc-discharge, laser ablation, and plasma radiation) [4–7] are mostly limited to solid state strategies that can tolerate relatively high energies and high temperatures [8]. Such methods have limitations, however, in terms of large-scale and economical production since they require extreme conditions and provide low yields. Carbon nanoparticles (CNPs) have been studied broadly for their use in adsorbents [9,10], composites [11], catalyst supports [12–16], and electronic materials [11] as well as in drug delivery [17,18], medical imaging [19], cell delivery [20], and cancer vaccination [21]. Furthermore, their large surface areas and ability to be functionalized allow them to undergo high-capacity binding to various biomolecules. Considering their wide spectrum of applications, the economical synthesis of CNPs remains an attractive challenge. Soot-based syntheses of CNPs have attracted increasing attention recently; for example, it has allowed the simple preparation of luminescent nanocarbons [22–24]. Zhang et al. [25] found that raw candle soot mixed with nafion exhibited good electrochemical activity. In addition, carbon materials obtained from oil seeds and fibrous plant materials can be used for the storage of hydrogen [26].

In this paper, we describe the synthesis of CNPs derived from castor oil soot and their subsequent surface functionalization with C═O groups upon treatment with HNO_3 at elevated temperature. We characterized these carbonyl-activated CNPs (OCNP) morphologically, spectrally, and voltammetrically. In addition, we demonstrated the feasibility of the activated CNPs for the use in electrocatalytic applications.

2. Experimental

2.1. Reagents

Castor oil was purchased from a local market. Dopamine (DA), ascorbic acid (AA), uric acid (UA), tyrosine, serotonin, nicotinamide adenine dinucleotide reduced dipotassium salt (NADH), potassium ferricyanide ($K_3Fe(CN)_6$), potassium phosphate monobasic, potassium phosphate dibasic and hexaammineruthenium (III) chloride ($Ru(NH_3)_6Cl_3$) were purchased from Sigma (St. Louis, MO, USA) and used as received. Dimethylformamide and nitric acid were of ACS-certified reagent grade. Deionized water (>18 MΩ cm) from a Direct-Q system (Millipore, Billerica, MA) was used to prepare all aqueous solutions. A 0.1 M phosphate buffer (PB, pH 7.4) prepared by mixing desired quantity of potassium phosphate monobasic and potassium phosphate dibasic was used for all electrochemical studies.

* Corresponding author. Tel.: +886 2 3366 4439; fax: +886 2 3366 4438.
E-mail address: jaho@ntu.edu.tw (J.-A.A. Ho).
[1] These authors contributed equally to this work.

0039-9140/$ – see front matter © 2011 Elsevier B.V. All rights reserved.
doi:10.1016/j.talanta.2011.10.056

2.2. Preparation of CNPs and OCNPs from castor oil soot

Caster oil is placed in a 50 ml glass beaker containing a cotton wick given with 1 cm residue in length above the oil surface. Castor oil soot was collected by sitting a glass plate on top of the smoldering castor oil. A portion (20 mg) of the soot was assembled (from the glass plate) and refluxed with 5 M HNO_3 for 12 h at 100 °C. Subsequently the acid-treated soot was centrifuged (16,000 rpm for 20 min) to obtain a back carbon precipitate. The as-obtained black precipitate (namely carbonyl-activated CNPs) was washed five times with water and then dried at 50 °C in an oven.

2.3. Fabrication of OCNP-modified electrodes

A coating solution was prepared by suspending 64 mg OCNP in 500 μL dimethylformamide which was subsequently sonicated for 20 min to ensure complete suspension of OCNPs. An aliquot (2 μL) of such suspension was dropped onto the working electrode surface of the screen-printed electrodes (SPEs) and dried overnight in an oven (50 °C). The OCNP-modified electrode (DOCNP) was then thoroughly rinsed with water to remove any loosely adsorbed particles. Coverage of OCNP on the SPE surface was evaluated by recording the peak current obtained from the cyclic voltammograms in 1 mM potassium ferricyanide solution.

2.4. Surface morphological and spectral studies

Surface morphologies were characterized using high-resolution transmission electron microscopy (TEM; JEOL, JEM-2100, Tokyo, Japan) and scanning electron microscopy (SEM; JEOL JSM-7000F, Tokyo, Japan). Fourier transform infrared (FTIR) spectroscopy and X-ray photoelectron spectroscopy (XPS) were performed using Spectrum One B (Perkin-Elmer, Waltham, MA, USA) and ULVACPHI XPS (model PHI Quantera SXM, Chigasaki, Japan) spectrometers, respectively. Zeta potentials were measured using a ZetaPlus zeta potential analyzer (Brookhaven, Holtsville, NY, USA).

2.5. Electrochemical analysis

Electrochemical measurements were performed at ambient temperature using a CHI 660B electrochemical workstation (Austin, Texas, USA). The SPEs, consisting of a carbon working electrode, a silver pseudo-reference electrode, and a carbon counter electrode, were purchased from Zensor R&D (Taichung, Taiwan).

3. Results and discussion

3.1. Characterization of surface morphology of CNPs

Because castor oil soot prepared in this study, consists no metal impurities, it becomes more hydrophilic after functionalization with HNO_3. Acid-treatment of carbonaceous particles typically results in major changes in their structural and functional properties [24,27]. The FTIR spectra (Fig. S1) of the acid-treated soot (OCNP) reveals the presence of surface CO_2H and C=O groups. The band at 1600–1700 cm^{-1} represents both C–OH and C=O bonds; the bands at 3100–3600 cm^{-1} indicate the presence of OH and CO_2H units. The acid-treated OCNPs possessed a negatively charged zeta potential of −30.47 mV, providing additional confirmation regarding the presence of CO_2H functionality on their surfaces. An XPS spectrum (Fig. 1) of the OCNPs reveals the presence of mainly carbon, oxygen, and nitrogen elements at 56.87, 31.92, and 11.21%, respectively. Based on the XPS survey scan, the O 1s/C 1s ratio was 0.56, providing additional direct evidence for the presence of surface C=O groups on the OCNPs. The data revealed more graphitic carbon at OCNP with oxygen/nitrogen bonded to carbon, apart

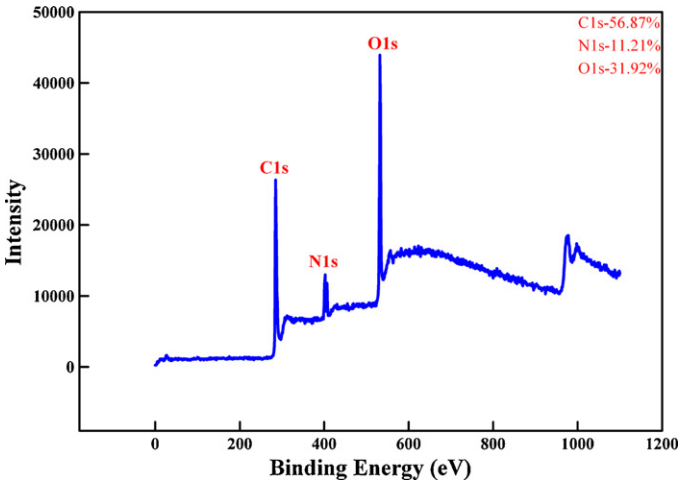

Fig. 1. XPS survey scan spectra for the OCNPs.

from this deconvoluted XPS (Fig. S2), it further gave more insights toward the surface functionalization, which were well matched with the observation obtained from the FTIR spectra. The deconvoluted spectrum for the C 1s energy level featured peaks at 284.5, 285.8, 288, and 290 eV, indicating the presence of graphitic carbon possessing C–OH, O–C=O and O–COO groups; in addition, the O 1s peaks at 531.7 and 533 eV were consistent with the presence of C=O and C–OH bonds. In the case of the N 1s energy levels, the peaks centered at 399.4, 401.4, and 406.2 eV were assigned to C–N and C=N functionalities and to some oxidized nitrogen species (e.g., N–O and/or N=O), respectively [27,28]. In addition, the C 1s peak at 284.5 eV represented sp^2-hybridized carbon atoms; the peak at 285.8 eV was assigned to sp^3 hybridization, suggesting the presence of defects in the CNPs [29]. The binding energy region between 285 and 286 eV was generally features the peaks of sp^3-hybridized carbon atoms and N–C(sp^2) atoms; the region between 286 and 230 eV referred to N–C(sp^3) carbon atoms and O–C=O groups [30]. The Raman spectra (Fig. 2) of the OCNPs revealed two distinct Raman bands at ca. 1330 cm^{-1} and ca. 1590 cm^{-1}; these bands, which are commonly attributed to the D (disorder/edge plane) and G (basal plane) bands, respectively. The D band at ca. 1330 cm^{-1} arose from the *k*-vector selection rule from reduced symmetry at graphite edge planes [31,32]. Our observation of a sharp and broad D band suggested the presence of "edge-plane-like" sites/defects similar to those of the outer graphene sheet of multiwalled carbon nanotubes (MWCNTs). The ratio of D and G bands was related to the degree of disorder and also to the degree of functionalization. The intensity ratio (I_D/I_G) in the spectrum of our CNP sample was greater than 1, inferring high degrees of disorder and functionalization. Taken together, all of our data (FTIR, XPS, and Raman

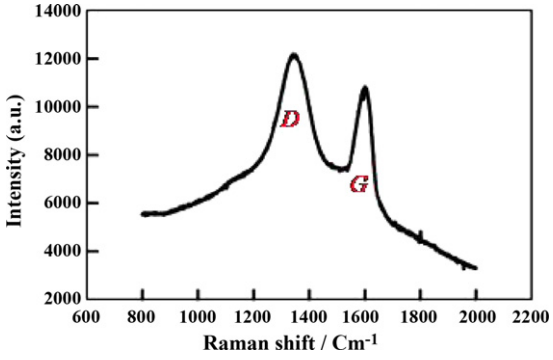

Fig. 2. Raman spectra of the OCNPs.

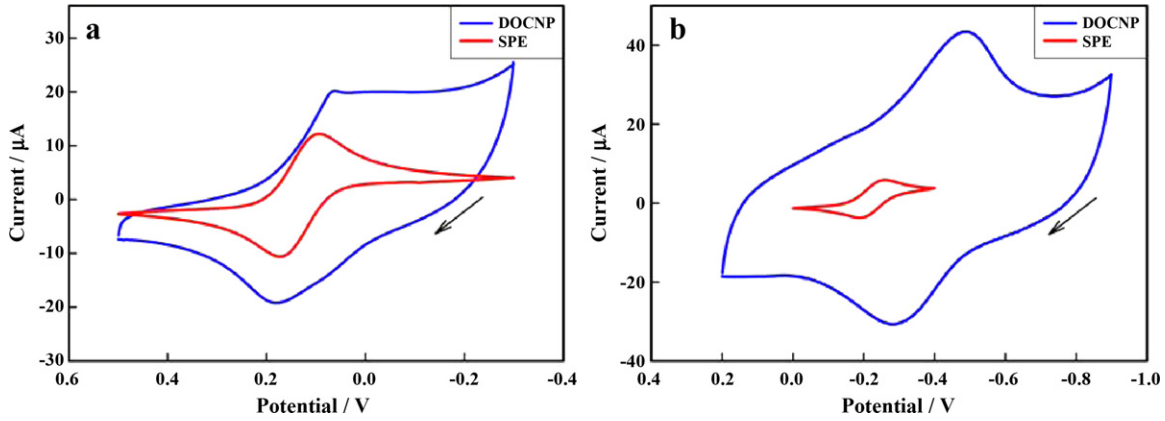

Fig. 3. Cyclic voltammograms of (a) 1 mM $K_3Fe(CN)_6$ in 0.1 M KCl and (b) 0.97 mM $Ru(NH_3)_6Cl_3$ in 0.1 M KCl recorded in the presence of the SPEs and DOCNP. Scan rate: 50 mV s^{-1}.

spectra; zeta potential) suggested the presence of surface functional groups and edge plane sites in the OCNPs. SEM and HR-TEM images (Figs. S3 and S4) of the acid-treated CNPs revealed that they were spherically shaped with particle sizes ranging from 38 to 75 nm.

3.2. Voltammetric characterization

We characterized the electrochemical activity of the DOCNP by studying its voltammetric behavior toward 1 mM potassium ferricyanide and 0.97 mM hexaaminеruthenium(III) chloride. For the potassium ferricyanide (Fig. 3a), the DOCNP exhibited a broad oxidation peak with a large capacitive background current while the reverse scan featured a triangle-like wave shape with a sharp reduction peak, akin to a stripping wave instead of a diffusion-controlled process. Similar behavior was observed in the acid-treated MWCNTs [33], suggesting that partial ferricyanide complex formed was reacting to the surface carboxyl or quinonyl groups. In the hexaammineruthenium (III) aspect, a further broad redox peaks and enhanced current were present with a potential shifting to less positive (−0.28 V for oxidation and −0.5 V for reduction), compared to those given by the bare SPEs. This result indicated the influence of both the edge plane defects and the surface functional groups of the acid-treated CNPs derived from castor

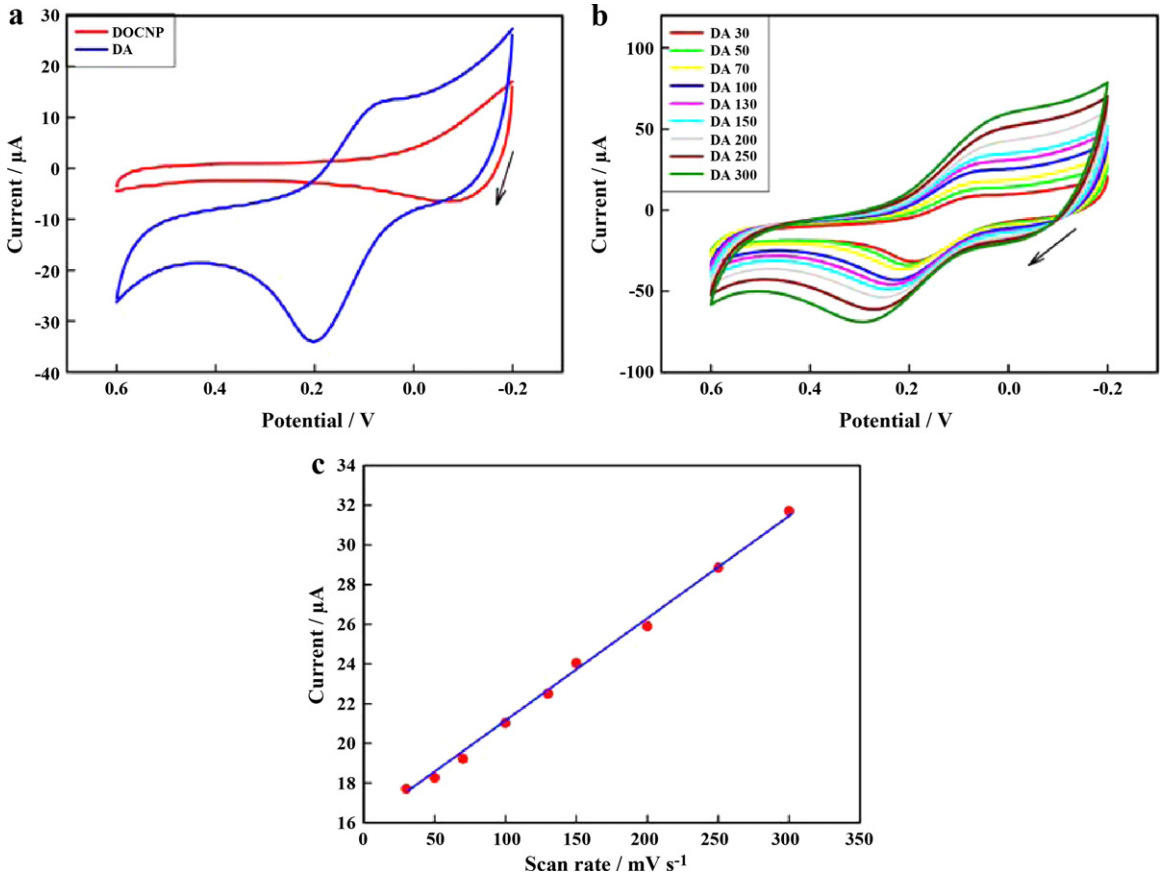

Fig. 4. (a) Cyclic voltammograms of 500 µM DA at DOCNP in 0.1 M PB (pH 7.4) (scan rate: 50 mV s^{-1}), (b) Cyclic voltammograms of DOCNP at scan rates ranging from 30 to 300 mV s^{-1}, (c) Linear relationship between the anodic peak current and the scan rate.

oil soot. Using potassium ferricyanide as a probe, we estimated the electroactive surface area based on the Randles–Sevcik equation:

$$I_p = (2.69 \times 10^5) n^{2/3} A D^{1/2} \nu^{1/2} Co$$

where I_p is the redox peak current, n is the number of electrons per molecule reduced or oxidized, A is the active surface area of the electrode surface (cm^2), D is the diffusion coefficient of potassium ferricyanide in 0.1 M KCl (0.76×10^{-6} cm^2 s^{-1}) [34], Co is the concentration of potassium ferricyanide, and ν is the scan rate ($V\,s^{-1}$). The active surface areas of the modified (DOCNP) and unmodified (bare) SPEs were 0.49 and 0.24 cm^2, respectively, indicating a 2-fold increase of active area on the DOCNP that yielded the enhanced current.

3.3. Electroanalytical application

In light of the high electrochemical activity of the DOCNP toward the typical redox substances observed in Fig. 3, we furthermore held evaluations toward numerous electroactive biomolecules. DA was selected as our sample of interest in feature of its significance in the medical field. Fig. 4 reveals the cyclic voltammograms of 500 μM DA recorded on DOCNP indicating obvious oxidation and reduction peaks at 200 and 75 mV, respectively. Compared to the CVs obtained from the unmodified SPE (shown in Fig. S5), the DOCNP exhibited substantially increased electrocatalytic current and enhanced reversibility. As illustrated in Fig. 4(a), DA is oxidized at 200 mV, less positive than 320 mV (on unmodified SPE depicted in Fig. S5, curve b) and 400 mV that previously reported [35]. On the other hand, the reduction peak of DA is explicit on the DOCNP, inferring the improved reversibility ascribable to an enhancement of electron transfer kinetics. Furthermore, we examined the cyclic voltammograms of DA on the DOCNP in connection to the scan rate from 30 to 300 mV s^{-1} (Fig. 4(b)) to reveal a linear relationship between the peck current and scan rate as shown in Fig. 4(c). The phenomenon infers that the oxidation of DA at the DOCNP occurred in an adsorption-determining manner. Such the adsorption-determining process was further evident from the voltammetric experiments performed in a relatively low concentration of DA (100 μM) with extended time of adsorption for 1 min. A pair of redox peaks arose legibly (shown as black curve in Fig. S6, denoted as 100DA after) indicating the effect of adsorption. In biological samples, AA generally co-exists with DA, but the oxidation potentials of AA and DA are too close to be determined separately using conventional electrodes. Therefore, we selected AA as a sample of interest; notably, the modified electrode exhibited no electrochemical oxidation behavior toward AA (Fig. 5), even at elevated concentrations of AA. Upon the addition of DA, the electrode

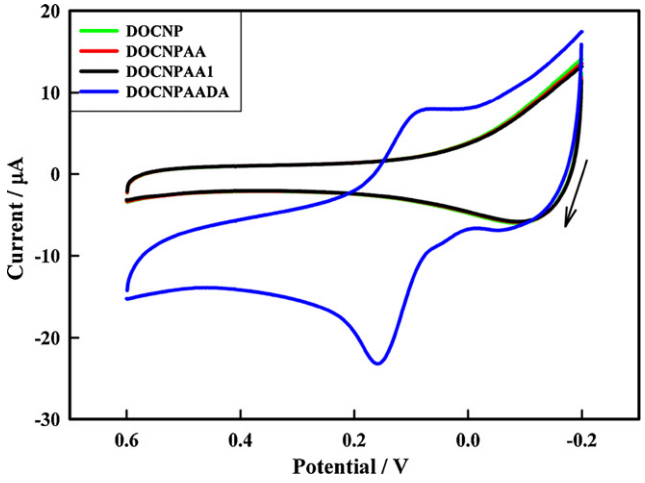

Fig. 5. Cyclic voltammograms of DOCNP at 500 μM (denoted as DOCNPAA) and 5 mM (denoted as DOCNPAA 1) AA, as well as further addition of 500 μM DA (denoted as DOCNPAAPA) in 0.1 M PB (pH 7.4). Scan rate: 50 mV s^{-1}.

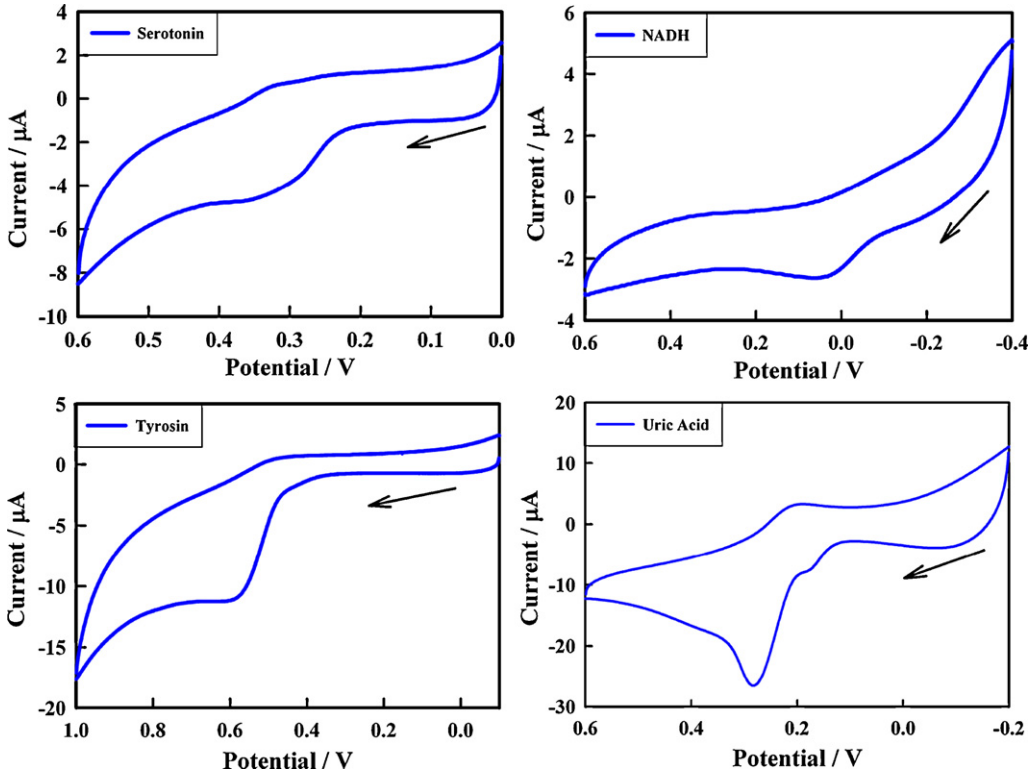

Fig. 6. Cyclic voltammograms of DOCNP in the presence of 600 μM serotonin, 1.8 mM tyrosine, and 3.4 mM UA (scan rate: 50 mV s^{-1}), as well as 500 μM NADH (scan rate: 10 mV s^{-1}) in 0.1 M PB (pH 7.4).

exhibited its typical redox behavior toward DA. This result suggests that the DOCNP is capable of selectively determining DA in the presence of AA in real samples of interest. We suspect that these phenomena might be due to the discrimination of the $>C(\delta+)=O(\delta-)$ electrode surface, as an opposing platform, to identify negatively charged functional groups [35], such as those of the anionic AA, at neutral pH. Our CNPs were highly functionalized with CO_2H groups after treatment with HNO_3; these units would electrostatically interact strongly with DA, with the edge plane defect enhancing the electron transfer rate and paving the way for much more negative potential for electrochemical oxidation. These observations are clearly consistent with the presence of surface functional groups and edge planes for the present CNPs.

Fig. 6 presents the voltammetric behavior of the biologically significant molecules: serotonin, NADH, tyrosine, and uric acid. Compared with the cyclic voltammograms given by bare SPE (Fig. S7), DOCNP exhibited greater electrocatalytic activity in term of reduced oxidation potential and obvious oxidation wave. The oxidation potentials were 330, 50, 590, and 280 mV characteristic to serotonin, NADH, tyrosine, and uric acid, respectively, giving less positive potential compared to those observed in bare SPEs. Note that NADH is oxidized at 50 mV exhibiting attractive feature of the castor oil soot-functionalized electrode, presumably due mainly to the surface C=O groups at the edge planes mediating the oxidation of NADH at the electrode surface.

Considering all of these observations, it appears that the surface functionality and edge planes of the OCNP played important roles influencing the electrochemical reactions of the various biologically important molecules. With the substantial reduction of potential to activate the oxidation of biomolecules (e.g., NADH) and enhanced electrocatalytic current, the DOCNP electrode holds the potential to mitigate the interference effect toward biosensing applications.

4. Conclusions

We have synthesized CNPs from castor oil soot through treatment with HNO_3 under reflux. Surface morphological, spectral, and voltammetric studies revealed the presence of surface functionalities and edge plane defects/sites and an increase in the electroactive surface area after acid treatment. An OCNP-modified electrode displayed greater electrocatalytic activity toward various biologically important molecules than did the unmodified electrode, presumably because of the edge plane defects/sites and surface C=O functionalities, the presence of which was supported by XPS, FTIR, and Raman spectral analyses. We suspect that this OCNP could be usefully applied for biosensing; current studies in our laboratory are focused on monitoring the neurotransmitter interactions of *Drosophila melanogaster* with such modified electrodes.

Acknowledgments

This study was supported by the National Science Council in Taiwan under grants NSC 95-2113-M-007-040-MY3 and 98J900026. We thank Dr. P. T. Joseph for the help in the XPS data analysis.

Appendix A. Supplementary data

Supplementary data associated with this article can be found, in the online version, at doi:10.1016/j.talanta.2011.10.056.

References

[1] S. Iijima, Nature 354 (1991) 56.
[2] N. Keller, N.I. Maksimova, V.V. Roddatis, M. Schur, G. Mestl, Y.V. Butenko, V.L. Kuznetsov, R. Schlögl, Angew. Chem. Int. Ed. 41 (2002) 1885.
[3] H.W. Kroto, J.R. Heath, S.C. O'Brien, R.F. Curl, R.E. Smalley, Nature 318 (1985) 162.
[4] I. Alexandrou, C.J. Kiely, A.J. Papworth, G.A.J. Amaratunga, Carbon 42 (2004) 1651.
[5] Z.H. Kang, E.B. Wang, L. Gao, S.Y. Lian, M. Jiang, C.W. Hu, L. Xu, J. Am. Chem. Soc. 125 (2003) 13652.
[6] X.M. Sun, Y.D. Li, Angew. Chem. Int. Ed. 43 (2004) 597.
[7] N.Q. Zhao, C.N. He, Z.Y. Jiang, J.J. Li, Y.D. Li, Mater. Lett. 60 (2006) 59.
[8] C.N.R. Rao, R. Seshadri, A. Govindaraj, R. Sen, Mater. Sci. Eng. Rep. 15 (1995) 209.
[9] Y. El-Sayed, T.J. Bandosz, Langmuir 21 (2005) 1282.
[10] Z.R. Yue, J. Economy, J. Nanopart. Res. 7 (2005) 477.
[11] M. Kato, M. Ishibashi, Carbon Nanoparticle Composite Actuators, 4th World Congress on Biomimetics, Artificial Muscles and Nano-Bio, 2008; Journal of Physics: Conference Series, 2008, p. 012003.
[12] H. Yoon, S. Ko, J. Jang, Chem. Commun. 14 (2007) 1468.
[13] F. Rodriguez-Reinoso, Carbon 36 (1998) 159.
[14] P. Oliveira, A.M. Ramos, I. Fonseca, A.B. do Rego, J. Vital, Catal. Today 102 (2005) 67.
[15] A. Valente, A.M.B. do Rego, M.J. Reis, I.F. Silva, A.M. Ramos, J. Vital, Appl. Catal., A 207 (2001) 221.
[16] F. Coloma, J. Narciso-Romero, A. Sepulveda-Escribano, F. Rodriguez-Reinoso, Carbon 36 (1998) 1011.
[17] S. Kim, E. Shibata, R. Sergiienko, T. Nakamura, Carbon 46 (2008) 1523.
[18] Y.H. Ma, S. Manolache, F.S. Denes, D.H. Thamm, I.D. Kurzman, D.M. Vail, J. Biomater. Sci. Polym. Ed. 15 (2004) 1033.
[19] Y.P. Sun, B. Zhou, Y. Lin, W. Wang, K.A.S. Fernando, P. Pathak, M.J. Meziani, B.A. Harruff, X. Wang, H.F. Wang, P.J.G. Luo, H. Yang, M.E. Kose, B.L. Chen, L.M. Veca, S.Y. Xie, J. Am. Chem. Soc. 128 (2006) 7756.
[20] A.H. Yan, B.W. Lau, B.S. Weissman, I. Kulaots, N.Y.C. Yang, A.B. Kane, R.H. Hurt, Adv. Mater. 18 (2006) 2373.
[21] H.A. Schriber, J. Prechl, H. Jiang, A. Zozulya, Z. Fabry, F.S. Denes, M. Sandor, in: Y. Kawai, H. Ikegami, N. Sato, A. Matsuda, K. Uchino, M. Kuzuya, A. Mizuno (Eds.), Industrial Plasma Technology: Applications from Environmental to Energy Technologies, Wiley-VCH Verlag GmbH & Co. KGaA, Weinheim, 2009, p. 141.
[22] H. Liu, T. Ye, C. Mao, Angew. Chem. Int. Ed. 46 (2007) 6473.
[23] L. Tian, D. Ghosh, W. Chen, S. Pradhan, X. Chang, S. Chen, Chem. Mater. 21 (2009) 2803.
[24] S.C. Ray, A. Saha, N.R. Jana, R. Sarkar, J. Phys. Chem. C 113 (2009) 18546.
[25] W. Zhang, G. Wang, N. Zhang, C. Zhang, B. Fang, Chem. Lett. 38 (2009) 28.
[26] M. Sharon, R. Soga, D. Afre, K. Sathiyamoorthy, S. Bhardwaj, M. Sharon, S. Jaybhaye, Int. J. Hydrogen Energy 32 (2007) 4238.
[27] T.I.T. Okpalugo, P. Papakostatinou, H. Murphy, J.A. McLaughlin, N.M.D. Brown, Carbon 43 (2005) 153.
[28] S.D. Gardner, G. He, C.U. Pittman Jr., Carbon 34 (1996) 1221.
[29] D.Y. Kim, C.M. Yang, H. Noguchi, M. Yamamoto, T. Ohba, H. Kanoh, K.K Kaneko, Carbon 46 (2008) 611.
[30] J.W. Jang, C.E. Lee, S.C. Lyu, T.J. Lee, C.J. Lee, Appl. Phys. Lett. 84 (2004) 2877.
[31] R. Bowling, R.T. Packard, R.L. McCreery, Langmuir 5 (1989) 683.
[32] K. Ray, R.L. McCreery, Anal. Chem. 69 (1996) 4680.
[33] A.F. Holloway, G.G. Wildgoose, R.G. Compton, L. Shao, M.L.H. Green, J. Solid State Electrochem. 12 (2008) 1337.
[34] N.R. Adams, Electrochemistry at Solid Electrodes, New York, Marcel Dekker, 1969 (Chapters 3 and 8).
[35] K.S. Prasad, G. Muthuraman, J.M. Zen, Electrochem. Commun. 10 (2008) 559.